# Phase stability and nondilute Li diffusion in spinel Li$_{1+x}$Ti$_2$O$_4$

Jishnu Bhattacharya[1] and Anton Van der Ven[2,*]

[1]*Department of Mechanical Engineering, The University of Michigan, Ann Arbor, Michigan 48109, USA*
[2]*Department of Material Science and Engineering, The University of Michigan, Ann Arbor, Michigan 48109, USA*

We report on a comprehensive first-principles investigation of Li diffusion in spinel Li$_{1+x}$Ti$_2$O$_4$, a viable anode material for Li-ion batteries. Concentration dependent diffusion coefficients are calculated by applying kinetic Monte Carlo simulations to a first-principles parametrized cluster expansion of the configurational energy and migration barriers. Diffusion mechanisms in spinel transition metal oxide intercalation compounds are sensitive to the Li concentration. Below $x=0$ in Li$_{1+x}$Ti$_2$O$_4$, Li ions occupy tetrahedral sites and individual Li hops between neighboring tetrahedral sites pass through intermediate octahedral sites, which we find to be activated states as opposed to local minima. The migration barriers are sensitive to the overall Li concentration, decreasing as the Li concentration over the tetrahedral sites is increased. A miscibility gap exists between LiTi$_2$O$_4$ and Li$_2$Ti$_2$O$_4$. Li-diffusion mechanisms in Li$_2$Ti$_2$O$_4$ are qualitatively different from those in Li$_{1+x}$Ti$_2$O$_4$ when $x<0$, with Li hops between neighboring octahedral sites passing through intermediate tetrahedral sites that are locally stable. The present study provides insight to the origin of the high Li mobility in spinel crystal structures compared to the layered crystal structures of common intercalation compounds used as electrodes in Li-ion batteries.

## I. INTRODUCTION

Charge and discharge rates of Li-ion batteries depend sensitively on Li-ion mobility within the electrode materials. Most electrode materials of reversible Li-ion batteries are intercalation compounds that accommodate Li ions in the interstitial sites of a crystalline host.[1] Lithium ions diffuse in and out of the intercalation compound by exchanging with vacancies. Often the Li concentration within the host can be varied from very dilute concentrations to the fully concentrated limit. Hence, Li diffusion predominantly occurs at nondilute concentrations where interactions among Li ions play an important role in influencing mobility.

Lithium intercalation compounds exhibit a wide variety of crystal structures and chemistries.[1–4] Transition metal oxides such as Li$_x$CoO$_2$, Li$_x$(Ni$_{1/2}$Mn$_{1/2}$)O$_2$, and Li$_x$(Co$_{1/3}$Ni$_{1/3}$Mn$_{1/3}$)O$_2$ have a layered crystal structure that accommodates Li ions between transition metal oxide slabs, thereby restricting Li diffusion to two-dimensional layers. Crystallographic features of the lithium sites in layered Li$_x$CoO$_2$ and Li$_x$TiS$_2$, for example, result in a diffusion mechanism predominantly mediated by divacancies,[5–7] which becomes inefficient at high Li concentrations where the number of vacancies becomes small. Diffusion in layered intercalation compounds is also affected by dimensional variations of the host crystal structure. The contraction of the $c$-lattice parameter (perpendicular to the Li layers) with decreasing Li concentration in Li$_x$CoO$_2$ and Li$_x$TiS$_2$ results in an increase of migration barriers, causing the diffusion coefficient to decrease at low Li concentration.[6,7] Intercalation compounds such as Li$_x$FePO$_4$ have an olivine crystal structure[8] in which Li diffusion is restricted to one-dimensional channels.[9] One-dimensional diffusion has important consequences for the rate capabilities of the olivine compounds as well as the kinetic mechanisms of the two-phase reaction from LiFePO$_4$ to FePO$_4$.[10–13] The crystal

structures of other intercalation compounds such as spinel Li$_x$Mn$_2$O$_4$ (Ref. 14) or anatase TiO$_2$ (Refs. 15 and 16) consist of three-dimensional interstitial networks, and it is generally believed that higher dimensional networks lead to enhanced Li mobility.

While several in-depth studies have been performed on Li diffusion in layered intercalation compounds,[6,7] much remains to be understood about the dependence of diffusion mechanisms on crystal structure and composition in nonlayered intercalation compounds. In this paper, we perform a first-principles investigation of lithium diffusion in the spinel crystal structure as a function of lithium concentration, focusing on Li$_{1+x}$Ti$_2$O$_4$.[17–19] The spinel form of Li$_{1+x}$Ti$_2$O$_4$ is crystallographically identical to spinel Li$_x$Mn$_2$O$_4$.[14,20] Though the manganese spinel variant is currently used as a cathode in Li-ion batteries for automotive applications, its electronic structure is significantly more complex than that of spinel Li$_{1+x}$Ti$_2$O$_4$, exhibiting localized charge ordering,[21] local and cooperative Jahn-Teller distortions,[22] and complex magnetic ordering,[23–25] all varying with Li concentration. The arrangements of Mn$^{3+}$ and Mn$^{4+}$ ions in spinel Li$_x$Mn$_2$O$_4$, for example, are likely correlated with the arrangements of Li ions and could result in a coupling between Li hops and rearrangements of charge ordering over the Mn sublattice. This electronic complexity is for a large part absent in Li$_{1+x}$Ti$_2$O$_4$, thereby simplifying the study of both its thermodynamic[26] and kinetic properties and allowing us to isolate the role of the spinel crystal structure on lithium diffusion at nondilute concentrations.

Unlike most lithium transition metal oxides that serve as cathodes in Li-ion batteries, the Li$_{1+x}$Ti$_2$O$_4$ spinel electrode exhibits a low voltage making it a viable anode in lithium batteries. Especially the Li-excess variant, Li$_{1+x}$(Li$_{1/6}$Ti$_{5/6}$)$_2$O$_4$, has proven very attractive as a high rate anode material[18,19,27–30] in part since its cubic lattice parameter varies negligibly with Li concentration, thereby making it less susceptible to mechanical fatigue that results from

repeated Li removal and insertion. The spinel titanate also operates above the voltage of solid-electrolyte interface formation, which is in part responsible for the limited cycle lifetimes of graphitic anodes.[31,32]

We start our study with an investigation of the thermodynamics of Li intercalation in $Li_{1+x}Ti_2O_4$ spinel from first principles using a cluster expansion in combination with Monte Carlo simulations. Next we analyze elementary Li hop mechanisms at a variety of Li compositions and in various states of Li-vacancy order or disorder. These results are then used in kinetic Monte Carlo simulations where Li-diffusion coefficients are calculated as a function of Li concentration. A cluster expansion is implemented in the kinetic Monte Carlo simulations to rigorously account for variations in the migration barriers with Li composition and local Li-vacancy (dis)order. We conclude with a discussion of the unique features of the spinel crystal structure with respect to Li diffusion and how they lead to enhanced mobility compared to layered intercalation compounds.

## II. METHODS

We use a combination of well-established electronic structure[33] and statistical mechanical techniques[34–37] to study phase stability and lithium transport as a function of lithium concentration. First-principles energies are used to parametrize a cluster expansion (i.e., an effective Hamiltonian) describing the energy of the crystal as a function of the configurational degrees of freedom arising from all possible ways of arranging Li ions and vacancies over the interstitial sites of the spinel $Ti_2O_4$ host. Contributions from electronic and vibrational degrees of freedom are less important in lithium intercalation compounds and are neglected in the present study. The cluster expansion is then used in Monte Carlo simulations to predict finite temperature phase stability. Lithium diffusion within the electrode material is a nonequilibrium kinetic process and therefore depends both on equilibrium properties of the solid as well as the manner in which it responds to small deviations from equilibrium. Kinetic Monte Carlo simulations applied to the cluster expansion enable the calculation of Li-diffusion coefficients using a Kubo-Green formalism. Below we describe the various techniques used in this study in more detail.

### A. First-principles calculations

Essential ingredients for the construction of a cluster expansion (effective Hamiltonian), to be used in Monte Carlo simulations, are the energies of different Li-vacancy arrangements over the $Li_{1+x}Ti_2O_4$ host as well as the migration barriers for Li-ion hops in different environments and Li concentrations. These were calculated with density functional theory (DFT) as implemented in the VASP plane wave electronic structure code.[38,39] We worked within the generalized-gradient approximation (GGA) and used projector augmented wave[40,41] pseudopotentials for the electronic core states. All calculations were performed nonspin polarized as several tests at three Li compositions spanning the whole composition range indicated that total energies are not af-

fected by the inclusion of spin polarization. Migration barriers for Li hops between adjacent sites were calculated with the nudged elastic band (NEB) method as implemented in VASP. The NEB calculations were performed at constant volume, fixing the volume to that of the initial state of the hop.

### B. Cluster expansion

The cluster expansion is a mathematical technique to parametrize any property of the crystal that depends on configurational degrees of freedom.[34,35,42] In spinel $Li_{1+x}Ti_2O_4$, configurational degrees of freedom arise from all $2^M$ possible ways of distributing Li ions and vacancies over the $M$ available tetrahedral and octahedral interstitial sites of the oxygen sublattice of the $Ti_2O_4$ host. A particular arrangement of Li ions and vacancies can be specified by assigning an occupation variable, $\sigma_i$, to each Li site $i$, which is $+1$ if it is occupied and $-1$ if it is vacant. The collection of all occupation variables $\vec{\sigma} = \{\sigma_1, \ldots, \sigma_i, \ldots, \sigma_M\}$ then uniquely determines the arrangement of Li ions within the crystal. A useful property of this description is that the products of occupation variables, $\sigma_i$, belonging to clusters of sites $\alpha$ (e.g., pair clusters, triplet clusters, etc.) and defined according to

$$\varphi_\alpha(\vec{\sigma}) = \prod_{i \in \alpha} \sigma_i, \qquad (1)$$

form a complete and orthonormal basis in configuration space.[34] Hence, any property of the crystal that depends on how its atoms are arranged on a particular lattice (e.g., Li and vacancies over the interstitial sites of spinel $Ti_2O_4$) can be expanded in terms of the basis functions $\varphi_\alpha$ according to[34]

$$E(\vec{\sigma}) = V_0 + \sum_\alpha V_\alpha \cdot \varphi_\alpha(\vec{\sigma}), \qquad (2)$$

where the $V_0$ and $V_\alpha$ are referred to as effective cluster interactions (ECIs). The above expansion is rigorous when the sum extends over all possible clusters of sites. The ECIs, which are constant and independent of composition, are not to be confused with interatomic potentials. They are expansion coefficients that describe the energy of the crystal as a function of the configuration of the Li ions and vacancies. In practice, the above cluster expansion must be truncated above some maximum sized cluster. The ECIs of the truncated cluster expansion can then be determined by fitting Eq. (2) to first-principles energies of a subset of all possible Li-vacancy configurations. The quality of the cluster expansion is usually measured by a root mean square error with respect to the energies of the Li-vacancy configurations used in the fit and a cross validation score, which measures the quality of the cluster expansion in predicting structures not included in the fit.[43] The quality of the fit can be controlled by the level of truncation of the cluster expansion. Here we use a genetic algorithm to find the optimal collection of clusters to include in the fit.[44]

A truncated cluster expansion can be evaluated rapidly for any configuration of Li ions and vacancies over the interstitial sites of the spinel host. Subjecting it to standard Monte Carlo simulations, within the grand canonical ensemble, for example, enables the calculation of thermodynamic proper-

ties, including the relationship between the Li chemical potential and the Li concentration. This relationship is of importance for battery applications as the open circuit voltage of an intercalation compound electrode with respect to a metallic Li reference anode is related to the chemical potentials of the electrodes according to

$$V(x) = -\frac{\mu_{\text{Li}} - \mu_{\text{Li}}^{reference}}{Fz}, \tag{3}$$

where $z$ is the electron charge carried by one Li ion, $F$ is Faraday's constant, and $\mu_{\text{Li}}$ is the Li chemical potential of the intercalation compound. $\mu_{\text{Li}}^{reference}$ is the Li chemical potential of a pure Li reference electrode.

### C. Calculation of diffusion coefficients

The diffusion coefficient, $D$, appearing in Fick's first law depends both on the thermodynamic as well as the kinetic properties of the solid. For Li diffusion over the interstitial sites of the host, it is convenient to write $D$ as a product of a thermodynamic factor, $\Theta$, and a self-diffusion coefficient, $D_J$, according to $D = \Theta D_J$.[45] The thermodynamic factor

$$\Theta = \frac{\partial\left(\dfrac{\mu_{\text{Li}}}{k_B T}\right)}{\partial \ln x} \tag{4}$$

measures the deviation from thermodynamic ideality. It is unity in the dilute limit where interactions between different Li ions are negligible and diverges close to an ordered stoichiometric phase where the deviation from ideal solution behavior is the largest. The self-diffusion coefficient measures the mobility of the Li ions over the interstitial sites and can be evaluated at equilibrium with a Kubo-Green expression[46]

$$D_J = \frac{1}{2dt}\frac{1}{N}\left\langle \left[ \sum_{i=1}^{N} \Delta R_i(t) \right]^2 \right\rangle, \tag{5}$$

where $d$ is the dimension of the interstitial lattice (for $\text{Li}_{1+x}\text{Ti}_2\text{O}_4$ spinel, it is three dimensional), $t$ is the time, $N$ is the total number of lithium ions, and $\Delta R_i(t)$ is the vector connecting the end points of the trajectory of the $i$th Li ion at time $t$. The self-diffusion coefficient, $D_J$, has a similar form as that of the tracer diffusion coefficient, $D^*$, which is defined as

$$D^* = \frac{1}{2dt}\frac{1}{N}\sum_{i=1}^{N} \langle [\Delta R_i(t)]^2 \rangle. \tag{6}$$

The self-diffusion coefficient is related to the square of the displacement of the center of mass of all diffusing Li ions at equilibrium, thereby accounting for correlations in the trajectories between different Li ions. The self-diffusion coefficient is therefore a measure of the collective mobility of many Li ions. The tracer diffusion coefficient, $D^*$, in contrast is related to the square of the displacement of one Li and therefore measures the mobility of individual Li ions. While $D_J$ and $D^*$ are metrics of the kinetics of diffusion, they also depend on the thermodynamic behavior of the solid. The

mobility of Li ions can be very sensitive to the equilibrium degree of short- and long-range order among the Li ions. Often mobility is reduced in ordered phases having stoichiometric compositions as elementary hops will then introduce some degree of local disordering, which is often accompanied by a significant increase in the energy of solid.

The thermodynamic factor [Eq. (4)] can be calculated with grand canonical Monte Carlo simulations by evaluating[45]

$$\Theta = \frac{\langle N \rangle}{\langle (\delta N)^2 \rangle}, \tag{7}$$

where $N$ is the number of Li atoms in the system (Monte Carlo cell) and $\delta N$ is the fluctuation around the average $\langle N \rangle$ at constant Li chemical potential $\mu_{\text{Li}}$. Both $D_J$ and $D^*$ can be calculated with kinetic Monte Carlo simulations, which simulate trajectories $\Delta R_i(t)$ as a function of time. Essential input for a kinetic Monte Carlo simulation[47,48] is an accurate description of hop frequencies for elementary Li-vacancy exchanges. These can be calculated with transition state theory, which for Li-ion hops into an adjacent vacant site takes the form[49]

$$\Gamma = \nu^* \exp\left(\frac{-\Delta E}{k_B T}\right), \tag{8}$$

where $\Delta E$ is the activation barrier and $\nu^*$ is the vibrational prefactor. Often the Li ions are disordered over the interstitial sites of the host and can sometimes exhibit long-range order at stoichiometric compositions. The migration barriers $\Delta E$ appearing in the hop frequency [Eq. (8)] depend on the local Li composition and state of disorder and will therefore vary as the migrating ions sample different local environments along their trajectories. Several approaches have been formulated and implemented to account for the dependence of migration barriers on local Li-vacancy disorder using a local-cluster expansion.[6,7] In this study, we also use a cluster expansion to describe the dependence of the migration barrier on the local degree of disorder.

### III. RESULTS

The spinel form of $\text{Li}_{1+x}\text{Ti}_2\text{O}_4$, which belongs to the $Fd\bar{3}m$ space group, consists of an oxygen fcc sublattice (32$e$ sites) with the titanium atoms filling half of the available octahedral interstitial sites of the oxygen sublattice (16$d$ sites). The other half of the octahedral sites, designated 16$c$, and one eighth of the available tetrahedral sites, designated 8$a$, can be occupied by Li.[4] The remaining interstitial sites share faces with oxygen octahedra surrounding titanium and are, therefore, energetically too costly for lithium occupancy. The crystal structure of spinel and the interstitial Li sites are shown in Fig. 1.

The tetrahedral 8$a$ sites form a diamond sublattice. The octahedral 16$c$ sites reside half-way between neighboring tetrahedral sites. Each tetrahedral site, therefore, has four octahedral nearest-neighbor sites, while each octahedral site has two nearest-neighbor tetrahedral sites. There are twice as many octahedral 16$c$ sites as tetrahedral 8$a$ sites.
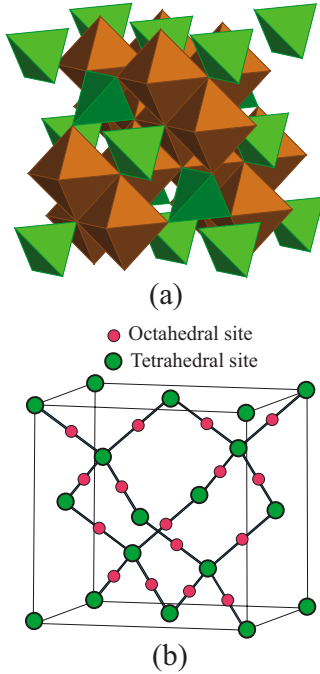
FIG. 1. (Color online) (a) Crystal structure of $Li_{1+x}Ti_2O_4$ spinel. Li ions can occupy the 8$a$ sites (center of the green $LiO_4$ tetrahedrons). Ti ions are located at the 16$d$ sites (center of the brown $TiO_6$ octahedrons). (b) The Li sublattice in the spinel host consists of a diamond network of 8$a$ tetrahedral sites (large green circles) with the octahedral 16$c$ sites (small pink circles) halfway in-between two nearest-neighbor tetrahedral sites.

### A. Formation energies and cluster expansion

To construct a cluster expansion for the configurational energy, we calculated the formation energies of 123 symmetrically nonequivalent lithium-vacancy configurations over the interstitial sites of the $Li_{1+x}Ti_2O_4$ spinel using DFT (VASP within GGA). Configurations were generated in periodic supercells having varying sizes. Fourteen configurations had the primitive unit cell consisting of four Ti and eight O atoms; 64 configurations had a supercell consisting of two primitive cells; 40 configurations had a cubic supercell consisting of four primitive cells; and five configurations had a supercell consisting of eight primitive cells ($2 \times 2 \times 2$). The coordinates of all atoms were fully relaxed. An energy cutoff of 400 eV was used and an $8 \times 8 \times 8$ $k$ point mesh was used in the reciprocal lattice of the primitive cell. For the cubic supercell and the supercell with eight primitive cells, we used a $4 \times 4 \times 4$ $k$-point grid. Of the 123 configurations investigated, 15 relaxed to other configurations, reducing the number of fully relaxed symmetrically distinct configurations to 108. The formation energies of these configurations were calculated with respect to the energies of delithiated spinel $Ti_2O_4$ (keeping the spinel symmetry) and fully lithiated $Li_2Ti_2O_4$ (with Li filling all octahedral 16$c$ sites) according to

$$E_{formation} = E - \frac{1}{2}(1+x)E_{Li_2Ti_2O_4} - \frac{1}{2}(1-x)E_{Ti_2O_4} \quad (9)$$

and are illustrated in Fig. 2 (the formation energies are per primitive cell, which contains four Ti and eight O).
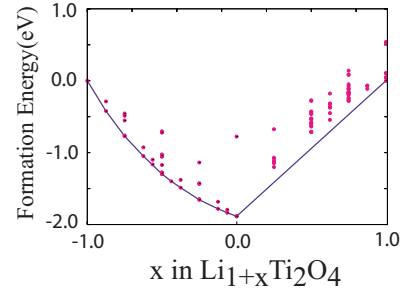


FIG. 2. (Color online) Formation energies of different configurations calculated from first-principles. The energies of the ground states are connected by the line forming a convex hull. Formation energies are per primitive cell consisting of four Ti and eight oxygen atoms.

The blue line in Fig. 2 represents the convex hull of the formation energies. The convex hull is equivalent to the well-known common tangent construction applied to free energies to determine phase stability as a function of composition. The formation energies residing on the convex hull in Fig. 2 are equal to the free energies of stable ordered phases of $Li_{1+x}Ti_2O_4$ at 0 K, where the entropy is equal to zero. The equilibrium state of $Li_{1+x}Ti_2O_4$ when $x$ has a value between pairs of stable ordered phases consists of a two-phase mixture of the two stable phases. The energy of the two-phase mixture resides on the common tangent at the composition $x$.

The DFT formation energies of Fig. 2 provide important insights about the behavior of Li insertion into spinel $Li_{1+x}Ti_2O_4$. In the concentration range $-1.0 < x < 0.0$, all low energy configurations consist of tetrahedral Li, in agreement with a previous first-principles study of this system.[26] Octahedral occupancy in the same composition range is mechanically unstable (see Sec. III C). Initial configurations with octahedral lithium either relax to a configuration with only tetrahedral occupancy or, if the symmetry of the configuration prevents Li relaxation out of an octahedral site, relax to a high-energy configuration corresponding to a saddle point in the energy landscape. At $x=1$, in contrast, the ground state structure consists of only octahedral Li ions. A miscibility gap (i.e., two-phase coexistence) exists in the range $0.0 < x < 1.0$ as can be seen by the absence of any ground states in that concentration range and as was predicted previously.[26]

The uniform and dense distribution of ground states for $-1.0 < x < 0.0$ suggests that a solid solution like behavior, where no particular ordering of lithium and vacancies is preferred, should dominate at moderate temperatures. This behavior changes once all tetrahedral sites of the host are occupied at $x=0$. For $x>0$, the configurations either consist of mixed tetrahedral and octahedral occupancy by Li or exclusively octahedral occupancy by Li. Although the energy of the crystal is minimized when Li occupies tetrahedral sites, the addition of Li to $LiTi_2O_4$, in which all the tetrahedral sites are filled, must occur by filling octahedral sites. This can occur in two ways: (i) if existing tetrahedral Li is not displaced, the additional Li must fill octahedral sites that are nearest neighbors to the filled tetrahedral sites, thereby incurring a large energy penalty; (ii) Li addition to octahedral sites can also be accompanied by the displacement of tetrahedral

Li to energetically less favorable but more abundant octahedral sites. In either case, the energy of the configuration with intermediate Li composition is higher than that of a two-phase mixture of $LiTi_2O_4$ and $Li_2Ti_2O_4$.

Experimentally, it is not possible to remove all the Li ions from spinel $Li_{1+x}Ti_2O_4$. Voltage curves have only been measured up to a composition of $x=-0.2$,[19] while studies using chemical delithiation indicate that Ti atoms begin to rearrange over the interstitial sites of the oxygen sublattice to adopt more stable arrangements as more and more Li are removed from spinel $LiTi_2O_4$.[50] The energy of delithiated spinel $Ti_2O_4$, for example, is higher than that of anatase $TiO_2$ by 557 meV/$TiO_2$ f.u. (both have the same fcc oxygen sublattice but a different Ti ordering over the octahedral sites). This shows that delithiated spinel has a significantly higher energy than other polymorphs of $TiO_2$ thereby making it susceptible to transformation. Even when the Ti atoms are constrained to remain in the 16$d$ sites of the spinel crystal structure, we found that the removal of symmetry constraints during total energy minimization of delithiated spinel $Ti_2O_4$ results in severe structural relaxations of the oxygen and titanium ions to the degree that it no longer resembles a spinel host structure.

Of the 108 symmetrically distinct configurations illustrated in Fig. 2, 70 were used to fit the ECIs of a cluster expansion for the configurational energy of Li-vacancy order or disorder over the tetrahedral and octahedral sites of $Li_{1+x}Ti_2O_4$. Two configurations in the dilute lithium regime were left out of the fit as they relaxed to structures that no longer resemble spinel while an additional 36 high-energy configurations were left out to facilitate a more rapid convergence of the truncated cluster expansion.[51] For statistical mechanical averaging, a key requirement of the cluster expansion is that it accurately predicts low energy configurations. We also fit to differences in energies between configurations in which a Li is initially in a tetrahedral site and then in an adjacent octahedral site. Since the octahedral sites are mechanically unstable when $x<0$, we used the nudged elastic band method to calculate the GGA saddle point energies of the octahedral sites. Fitting to differences in energy between octahedral and tetrahedral Li occupancies was done to ensure an accurate prediction of migration barriers since as will be described in Sec. III C, the octahedral sites correspond to activated states when $x<0$. Nine such differences in energy were used in the cluster expansion fit. The resulting cluster expansion consists of an empty cluster $V_0$, two point clusters (one for the tetrahedral and the other for the octahedral site), nine pair clusters, seven triplets, and five quadruplets. The overall rms error was 9 meV and the $CV$ score was 18 meV/$TiO_2$ f.u.

### B. Thermodynamics

Grand canonical Monte Carlo simulations were applied to the cluster expansion to calculate thermodynamic averages. We used 6000 Monte Carlo passes of which the first 2000 passes were for equilibration and the last 4000 were used for averaging. Each Li site is visited on average once during a Monte Carlo pass. Output from grand canonical Monte Carlo
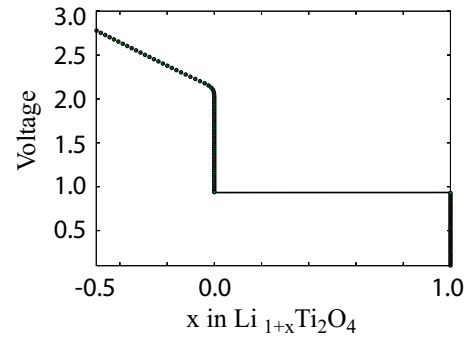


FIG. 3. (Color online) Equilibrium voltage curve as a function of lithium concentration (at room temperature), calculated with grand canonical Monte Carlo simulations. The plateau between $x=0.0$ and $x=1.0$ indicates two-phase coexistence.

simulations includes the equilibrium Li composition and average grand canonical energy as a function of chemical potential and temperature. Figure 3 shows the calculated voltage curve for $Li_{1+x}Ti_2O_4$ as a function of $x$ obtained by inserting the calculated chemical potential into Eq. (3) and using the energy of bcc Li for the chemical potential of the reference anode.

The plateau in the voltage curve signifies a two-phase coexistence between $LiTi_2O_4$ and $Li_2Ti_2O_4$. We will refer to $Li_{1+x}Ti_2O_4$ with $x<0$ as the $\alpha$ phase and $Li_{1+x}Ti_2O_4$ with $x \sim 1$ as the $\beta$ phase. The smooth decrease in voltage with increasing Li content in the $\alpha$ phase indicates solid solution behavior as expected from the first-principles formation energies. The plateau voltage is approximately 0.94 V, while the experimental voltage curve[19] exhibits a plateau at 1.34 V. The discrepancy can be attributed to the underestimation by GGA of voltages in transition metal oxide intercalation compounds due to self-interaction in the $d$ orbitals of the transition metals.[52] The step in the voltage at $x=0$ is approximately 1.2 V. Colbow $et$ $al.$[19] measured the voltage curve of $Li_{1+x}Ti_2O_4$ down to a Li concentration of $x=-0.2$. Their measured voltage curves indicate that the voltage increases by approximately 1.4 V when charging $Li_{1+x}Ti_2O_4$ from the plateau voltage to $x=-0.2$. The corresponding difference in the calculated voltage curve is 1.2 V. Apart from a systematic underprediction of the equilibrium voltage curve, both the qualitative shape and the relative variation in voltage are in very good agreement with experiment.

A phase diagram, mapping phase stability as a function of temperature and composition, can also be constructed based on output from Monte Carlo simulations. Using well-established free energy integration techniques[53] [i.e., $dG = \mu dN$ at constant $T$ and $d(\beta\Phi)=\Omega d\beta$ at constant $\mu_{Li}$, where $G$ is the Gibbs free energy, $\Phi=G-\mu_{Li}N$, $\Omega=E-\mu_{Li}N$, and $\beta=1/k_BT$], it is possible to calculate the Gibbs free energy as a function of composition at various temperatures. Regions of two-phase coexistence can then be determined with the common tangent construction applied to the Gibbs free energy (or equivalently by determining the crossing of $\Phi$'s for different phases as a function of $\mu_{Li}$). Free energy integration, however, requires a value for the free energy in a particular reference state. Convenient reference states correspond to those in which the configurational entropy is
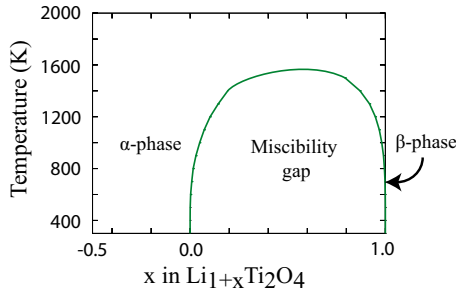
FIG. 4. (Color online) Calculated phase diagram as a function of temperature and lithium concentration. For low to moderate temperature, Li ions occupy tetrahedral sites for $x < 0.0$ ($\alpha$ phase). Li ions occupy octahedral sites at $x = 1.0$ ($\beta$ phase). There is a miscibility gap between the two phases for $0.0 < x < 1.0$. The miscibility gap disappears above 1500 K.

negligible, such as at dilute concentration and well-ordered phases at low temperature. The free energy of the phase is then very close to its energy and can be approximated with a low-temperature expansion technique.[54]

Figure 4 shows the calculated phase diagram for $Li_{1+x}Ti_2O_4$, which exhibits a miscibility gap between the $\alpha$ phase (with exclusively tetrahedral occupancy) and the $\beta$ phase (with exclusively octahedral occupancy). The equilibrium concentrations of the coexisting phases at fixed temperature define the boundary of the miscibility gap. The steep nature of the two-phase boundary suggests that both phases are very stable even at high temperatures until the system forms a complete solid solution above 1500 K.

The thermodynamic factor ($\Theta$) is an important part of the chemical diffusion coefficient and can be calculated in grand canonical Monte Carlo simulations by keeping track of the fluctuations of the number of lithium atoms at constant $\mu_{Li}$ according to Eq. (7). Figure 5 shows the variation of the thermodynamic factor with Li concentration at room temperature. In the $\alpha$ phase, $\Theta$ ranges between 20 and 40 but diverges as $x$ approaches 0 in $Li_{1+x}Ti_2O_4$ when all tetrahedral Li sites are filled. The thermodynamic factor also diverges in $\beta$-$Li_2Ti_2O_4$ in which all octahedral Li sites are occupied. Both $LiTi_2O_4$ and $Li_2Ti_2O_4$ correspond to well-ordered phases and therefore deviate strongly from thermodynamic ideality. In stoichiometric phases, with a dilute concentration of vacancies over the occupied sublattice, it can be shown
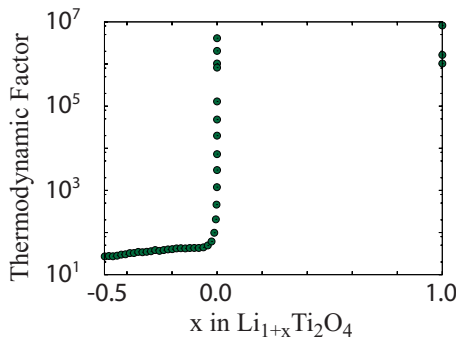


FIG. 5. (Color online) Variation of thermodynamic factor ($\Theta$) as a function of lithium composition. Note that the thermodynamic factor diverges near the stoichiometric phases ($x = 0.0$ and $x = 1.0$).

that the thermodynamic factor scales with the inverse of the vacancy composition. The thermodynamic factor is not defined in the two-phase region ($0 < x < 1$).

### C. Diffusion

#### 1. Elementary hop mechanisms and barriers

The mechanisms of lithium diffusion are qualitatively very different in the $\alpha$ and $\beta$ phases due to the change in Li site occupancy from tetrahedral sites in $\alpha$-$Li_{1+x}Ti_2O_4$ ($x < 0$) to octahedral sites in $\beta$-$Li_2Ti_2O_4$. Furthermore, as diffusion typically occurs in the nondilute concentration regime, interactions between nearby diffusing lithium ions also affect migration barriers for a particular atomic hop mechanism. We explored hop mechanisms and migration barriers from first-principles as a function of Li concentration using the NEB method as implemented in VASP. NEB calculations were performed within a cubic supercell of $Li_{1+x}Ti_2O_4$ containing 32 oxygen, 16 titanium, and variable number of lithium ions. Migration barriers were also calculated in larger supercells containing 64 oxygen, 32 titanium, and variable Li ions.

Figure 6(a) shows the lithium ion migration path as it hops between two nearest-neighbor tetrahedral sites. Figure 6(b) shows the energy along the migration path between adjacent tetrahedral Li sites in representative Li-vacancy configurations at three different concentrations ($x = -7/8$, $-1/2$, $-1/8$) in the $\alpha$ phase (i.e., Li occupies the tetrahedral sites). A Li hop between neighboring tetrahedral sites must pass through an octahedral site. The curve at $x = -1/2$, for example, is for a Li hop in one of many possible Li-vacancy configurations within the cubic unit cell used for these calculations. A striking feature of all three curves is that the octahedral site is never a local minimum but rather a saddle point (i.e., a maximum along the hop direction and a minimum perpendicular to the hop direction) for all compositions considered in the $\alpha$ phase ($-1 < x < 0$). This is contrary to the common belief that the octahedral sites of spinel intercalation compounds, such as $Li_{1+x}Mn_2O_4$ and $Li_{1+x}Ni_{0.5}Mn_{1.5}O_2$, while energetically less favorable than tetrahedral sites for $x < 0$, are nevertheless a local minimum.[4] The results of Fig. 6(b) show that this is not the case for $Li_{1+x}Ti_2O_4$, rather the octahedral site is the activated state of the hop. This is in agreement with recent NMR evidence on Li-excess spinel titanate.[55] Figure 6(b) also shows a variation of the migration barrier with Li concentration, systematically decreasing as the Li concentration increases. This is also illustrated in Fig. 6(c), which shows the migration barriers at seven different concentrations in $\alpha$-$Li_{1+x}Ti_2O_4$. At each concentration, there are many possible Li-vacancy configurations. In Fig. 6(b) we have only considered one configuration at each concentration; however, there will be some variability in migration barriers for different Li-vacancy configurations even at the same Li concentration. Overall, though, Fig. 6(c) shows a clear trend of decreasing migration barriers with increasing Li concentration. We point out that at very dilute Li concentrations (i.e., $x = -15/16$), large relaxations within the $2 \times 2 \times 2$ supercell resulted in a structure that no longer resembles the spinel host. The migration barrier cal-

(a)



(b)
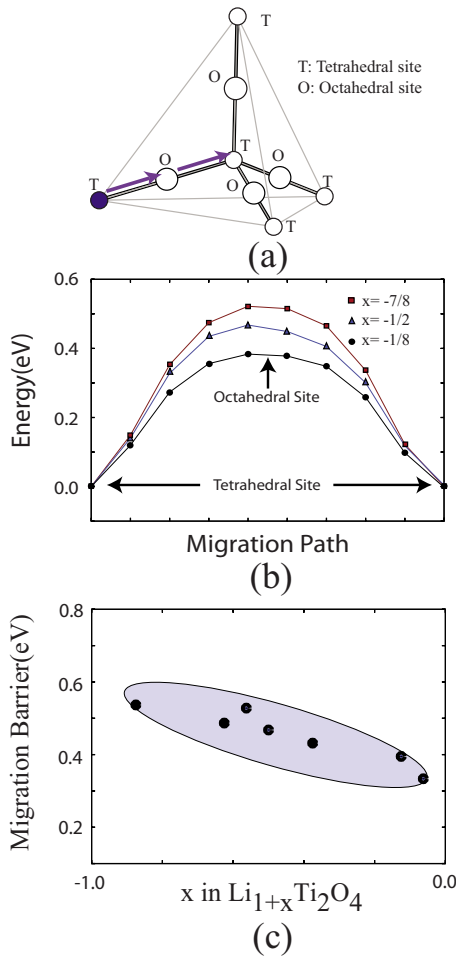
FIG. 6. (Color online) Migration barrier for different lithium concentrations in the $\alpha$ phase ($x<0$). (a) Lithium ion path during a hop (shown by the arrow) between two tetrahedral sites (marked as "T") through the intermediate octahedral site (marked as "O"). (b) Change in energy as a Li-ion hops in a particular configuration for three lithium compositions (Red squares: $x=-7/8$; blue triangles: $x=-1/2$; and black circles: $x=-1/8$.) (c) Trend of migration barriers with lithium composition.

culated at this concentration is not included in Fig. 6(c).

Li diffusion in $\beta$-Li$_2$Ti$_2$O$_4$ is qualitatively different from that in $\alpha$-Li$_{1+x}$Ti$_2$O$_4$ ($x<0$) as Li occupies octahedral sites now. The grand canonical Monte Carlo simulations (Sec. III B) indicate that $\beta$-Li$_2$Ti$_2$O$_4$ is only stable in a very narrow concentration interval. Hence diffusion will be primarily mediated by a dilute concentration of vacancies. Occasionally though, several vacancies may encounter each other, thereby forming vacancy complexes that result in diffusion mechanisms differing from that of a single vacancy hop mechanism. With the nudged elastic band method, we investigated two types of hops: (i) the migration of an octahedral Li to a neighboring vacant octahedral site [Fig. 7(a)] and (ii) the migration of an octahedral Li to a neighboring vacant octahedral site that is next to a second octahedral vacancy [Fig. 7(b)]. A Li ion migrating between nearest-neighbor octahedral sites must perform a curved hop through an adjacent tetrahedral site as illustrated in Figs. 7(a) and 7(b).



(c)
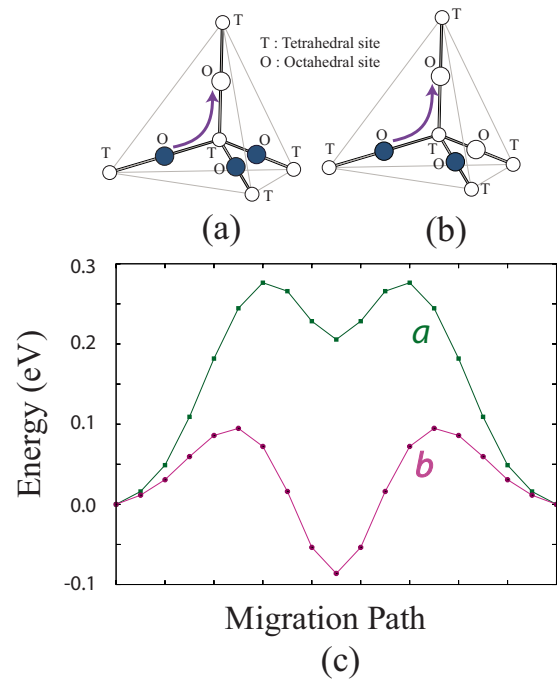
FIG. 7. (Color online) Migration energy barrier for different hop environments in $\beta$ phase. (a) Lithium ion path for a hop with a single vacancy. Octahedral sites are marked as O and tetrahedral sites are marked as T. Blue circles represent occupied octahedral sites and vacant octahedral sites are hollow circles. The hop path is shown by the set of arrows. (b) Lithium ion path for a hop with two octahedral vacancies. Color codes are the same as in (a). (c) Change in energy along the path for a hopping lithium ion in the neighborhood of single vacancy [green squares at the top, curve (a)] and in the neighborhood of two vacancies [pink circles at the bottom, curve (b)].

Figure 7(c) shows the calculated energy along the migration paths for the two hops of Figs. 7(a) and 7(b) as calculated with the NEB method. Curve $a$ in Fig. 7(c) (green squares) corresponds to the energy path when an octahedral lithium hops to a neighboring octahedral vacancy through an intermediate tetrahedral site. The tetrahedral site is a local minimum but higher in energy ($\sim$200 meV) compared to the octahedral site. The migration barrier for the octahedral to tetrahedral Li hop is $\sim$280 meV, while for the tetrahedral to octahedral hop, it is $\sim$80 meV. When there are two vacancies in nearest-neighbor octahedral sites, the energy curve changes substantially [curve (b) in Fig. 7(c)]. The tetrahedral site now becomes more stable than the octahedral site ($\sim$90 meV). As a result, the migration barrier for the octahedral to tetrahedral hop is lower ($\sim$100 meV) than that for the tetrahedral to octahedral hop ($\sim$190 meV). Both of the migration barriers were calculated in the same cubic cell used for most of the barrier calculations in $\alpha$ phase.

The local stability of the intermediate tetrahedral sites in $\beta$-Li$_2$Ti$_2$O$_4$ in the presence of octahedral single and divacancies implies that hops between neighboring octahedral sites occur as a sequence of two subhops (octahedral $\rightarrow$ tetrahedral and tetrahedral $\rightarrow$ octahedral). This is in contrast to hops between tetrahedral sites in $\alpha$-Li$_{1+x}$Ti$_2$O$_4$ ($x<0$) where, as described above, the intermediate octahedral
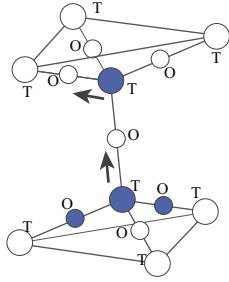
FIG. 8. (Color online) An example of a simultaneous two-atom simultaneous hop. Octahedral sites are marked as O and tetrahedral sites are marked as T. Blue circles represent occupied octahedral sites and vacant sites are hollow circles. Two arrows indicate simultaneous hops of two atoms.

sites are the activated states (i.e., saddle points).

When three octahedral vacancies in $\beta$-Li$_2$Ti$_2$O$_4$ encounter each other, the energy landscape becomes even more complex. We found that a configuration consisting of three octahedral vacancies surrounding a common vacant tetrahedral site is mechanically unstable: the fourth nearest-neighbor octahedral lithium of the vacant tetrahedral site spontaneously relaxes to the tetrahedral vacant site. This implies that once three octahedral vacancies coalesce, tetrahedral occupancy occurs spontaneously. Migration of this tetrahedral Li, however, cannot occur by means of a nearest-neighbor tetrahedral to octahedral hop since the end state of this hop is mechanically unstable. One possible mechanism with which a tetrahedral Li surrounded by four octahedral vacancies in $\beta$-Li$_2$Ti$_2$O$_4$ can migrate is through a coordinated two-atom hop as illustrated in Fig. 8. We did not investigate these possibilities in detail and restrict our analysis to octahedral to tetrahedral hops in the immediate vicinity of single octahedral vacancies and pairs of octahedral vacancies.

### 2. Kinetic Monte Carlo simulations

Having established the elementary hop mechanisms in $\alpha$-Li$_{1+x}$Ti$_2$O$_4$ and in stoichiometric $\beta$-Li$_2$Ti$_2$O$_4$, we next calculated collective Li-diffusion coefficients with kinetic Monte Carlo simulations. The kinetic Monte Carlo simulations sample Li trajectories over the interstitial sites of the Ti$_2$O$_4$ spinel host structure, whereby each elementary hop occurs with a frequency given by transition state theory according to Eq. (8). At nondilute concentrations, the Li ions and vacancies in $\alpha$-Li$_{1+x}$Ti$_2$O$_4$ are disordered, such that the migration barriers, $\Delta E$, appearing in Eq. (8) will vary along the trajectory of each Li ion as they depend on the local arrangement of Li ions and vacancies surrounding the Li performing a hop. In $\alpha$-Li$_{1+x}$Ti$_2$O$_4$, the migration barrier for elementary hops between neighboring tetrahedral sites is the difference in energy between the intermediate octahedral site and the initial tetrahedral site. These energy differences can be calculated directly with the cluster expansion for the configurational energy described in Sec. III A. The cluster expansion predicts the configurational energy over both the tetrahedral and octahedral sites of spinel Li$_{1+x}$Ti$_2$O$_4$ and, as described in Sec. III A, was optimized to reproduce energy

differences between octahedral and tetrahedral site occupancies.

In $\beta$-Li$_2$Ti$_2$O$_4$, both octahedral and tetrahedral sites correspond to local minima and elementary hops occur between adjacent octahedral and tetrahedral sites. In this case, the cluster expansion can only be used to predict the end states of the hop. To calculate the migration barriers within kinetic Monte Carlo in $\beta$-Li$_2$Ti$_2$O$_4$, we used a method that relies on a cluster expansion for the energies of end states of a hop combined with a kinetically resolved activation barrier, $\Delta E_{KRA}$, as described in Ref. 6. The $\Delta E_{KRA}$ for a given hop mechanism corresponds to the average of the forward and backward migration barriers. The actual migration barrier in a particular direction is then equal to $\Delta E_{KRA}$ plus the average of the end-state energies minus the energy of the initial state. The dependence of $\Delta E_{KRA}$ on the configuration of surrounding Li ions can be described with a local-cluster expansion.[6] In our kinetic Monte Carlo simulations of diffusion in $\beta$-Li$_2$Ti$_2$O$_4$, we only considered dilute vacancy concentrations (i.e., one vacancy or two vacancies in the Monte Carlo cell) such that the degree of disorder around migrating Li ions is minimal. In our simulations, we simply used a constant value for $\Delta E_{KRA}$ (162 meV) for a octahedral-tetrahedral hop surrounded by an isolated octahedral vacancy and a different value for $\Delta E_{KRA}$ (143 meV) for a octahedral-tetrahedral hop surrounded by an octahedral divacancy.

The vibrational prefactors, $\nu^*$, appearing in Eq. (8) were calculated within the local harmonic approximation.[56] Any variation of $\nu^*$ with concentration and configuration was not taken into account in this study. In $\alpha$-Li$_{1+x}$Ti$_2$O$_4$, we calculated $\nu^*$ for a lithium hop into an isolated vacancy within the cubic cell (1/8 vacancies over the tetrahedral sites). We used this value of $\nu^*$ (13.4 THz) over the whole composition range in the kinetic Monte Carlo simulations of $\alpha$-Li$_{1+x}$Ti$_2$O$_4$. In $\beta$-Li$_2$Ti$_2$O$_4$, we calculated $\nu^*$ for a octahedral to tetrahedral hop next to a single vacancy among 16 octahedral sites in the cubic cell. The vibrational prefactor was averaged over the forward and backward hop directions (octahedral$\rightarrow$tetrahedral and tetrahedral$\rightarrow$octahedral). This averaged value (5.9 THz) was used in the kinetic Monte Carlo simulations for $\beta$-Li$_2$Ti$_2$O$_4$.

We calculated the self- and tracer diffusion coefficients described in Sec. II C by simulating representative Li-ion trajectories in kinetic Monte Carlo simulations. We used a standard kinetic Monte Carlo algorithm, first proposed by Bortz et al.[47,48] A lithium-vacancy configuration representative of the equilibrium state at the temperature and composition of interest was chosen as the initial state of each simulation. For the $\alpha$ phase (Li$_{1+x}$Ti$_2$O$_4$; $x<0$), we used a Monte Carlo cell containing $8\times8\times8$ primitive cells (containing 3072 tetrahedral and octahedral sites). 3000 Monte Carlo passes were performed starting from each initial configuration and the trajectories were averaged after 1000 passes (each Monte Carlo pass corresponds to $N$ Li hops where $N$ is the number of Li sites). At each temperature and composition, 100 independent simulations were performed starting from different initial Li-vacancy configurations. At each temperature and composition, self- and tracer-diffusion coefficients [as described in Eqs. (5) and (6)] were averaged after every Monte Carlo pass and over independent simulations with different initial configurations.
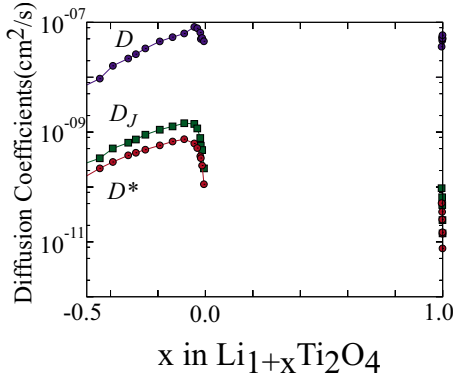
FIG. 9. (Color online) Calculated diffusion coefficients as a function of lithium composition. Red circles: tracer diffusion coefficient ($D^*$); green squares: self-diffusion coefficient ($Dj$); and purple circles: chemical diffusion coefficient ($D$).

For the stoichiometric $\beta$ phase ($Li_2Ti_2O_4$), we calculated diffusion coefficients using kinetic Monte Carlo cells containing either one octahedral vacancy or two octahedral vacancies. In the simulations containing two vacancies, we found that a fraction of the hops proceeds through the divacancy mechanism illustrated in Fig. 7(b) in which the intermediate tetrahedral occupancy is energetically more favorable than the octahedral end states [Fig. 7(c)]. The remaining hops proceeded as isolated single vacancy hops. The fraction of divacancy hops depends on the vacancy concentration, which we varied by changing the kinetic Monte Carlo cell size. We found, for example, that approximately 16% of the hops occurred according to the divacancy mechanism for a vacancy concentration of 0.23%, 10% for a vacancy concentration of 0.1%, and 7% for vacancy concentration of 0.05%. These vacancy concentrations over the octahedral sites of $\beta$-$Li_2Ti_2O_4$ correspond to Li concentrations that are within the predicted two-phase miscibility gap of the phase diagram of Fig. 4, indicating that the fraction of divacancy hops in stoichiometric $\beta$-$Li_2Ti_2O_4$ is small. By adjusting the kinetic Monte Carlo cell size (to sample different vacancy concentrations), we determined that both the tracer and self-diffusion coefficients scale linearly with vacancy concentration even for the simulations that contained two octahedral vacancies.

Figure 9 illustrates the calculated diffusion coefficients as a function of lithium concentration at room temperature. The chemical diffusion coefficient, $D$, was calculated by multiplying the self-diffusion coefficient, $D_J$, with the thermodynamic factor, $\Theta$ (of Fig. 5). All three diffusion metrics increase with increasing concentration in $\alpha$-$Li_{1+x}Ti_2O_4$ except as the Li concentration approaches $x=0$. The increase of $D^*$ and $D_J$ in $\alpha$-$Li_{1+x}Ti_2O_4$ has its origin in the gradual lowering of the migration barriers with Li concentration, as is predicted with DFT calculations described in Sec. III C 1 [Fig. 6(c)] and reproduced by the cluster expansion used in the kinetic Monte Carlo simulations. As the stoichiometric composition of $LiTi_2O_4$ is approached, however, $D^*$ and $D_J$ decrease sharply due to the reduction in the number of tetrahedral vacancies. The tracer diffusion coefficient is always less than the self-diffusion coefficient. Close to stoichiometric compositions (i.e., $LiTi_2O_4$ and $Li_2Ti_2O_4$), both $D^*$ and $D_J$
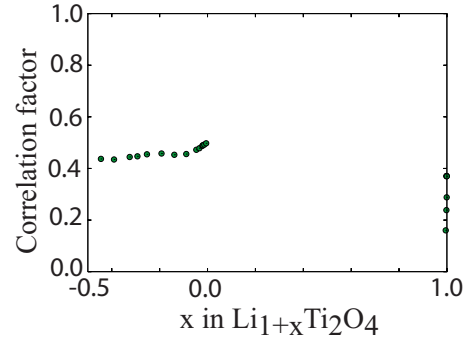


FIG. 10. (Color online) Variation of the correlation factor with lithium composition.

scale with the vacancy concentration, while the thermodynamic factor scales with the inverse of the Li-sublattice vacancy concentration. The dependencies of $D_j$ and $\Theta$ on vacancy concentration in stoichiometric phases cancel each other out when the self-diffusion coefficient and thermodynamic factor are multiplied together to obtain the chemical diffusion coefficient ($D$). Note that the chemical diffusion coefficients have very similar values in the $\alpha$ and $\beta$ phases in spite of the fact that the Li hop mechanisms are very different in the two phases.

The correlated motion of lithium ions at nondilute Li concentrations can be measured with the correlation factor, $f$, which is defined as

$$f = \frac{\langle \vec{r}(t)^2 \rangle}{na^2}, \qquad (10)$$

where $\langle \vec{r}(t)^2 \rangle$ is the average of the squared distance a lithium ion travels after a time $t$, $n$ is the number of hops, and $a$ is the hop distance. The correlation factor, $f$, measures the degree with which the actual Li tracer diffusion coefficient ($D^*$) deviates from what it would be if Li ions performed a random walk. The correlation factor is equal to 1 when subsequent Li hops are uncorrelated, as occurs in the dilute limit. However, at nondilute Li concentrations, Li ions interact with each other energetically and block potential sites for hops to occur to, thereby introducing correlations between successive Li hops. Figure 10 illustrates the calculated variation of the correlation factor, $f$, with lithium composition at room temperature. Compaan and Haven analytically calculated the correlation factor in the diamond crystal to be 0.5 in the presence of a single vacancy.[57] Figure 10 shows that $f$ is slightly less than 0.5 between $-0.5 < x < 0$, becoming equal to 0.5 as $x$ approaches 0, where the vacancy concentration over the tetrahedral sites goes to zero. The correlation factor in the $\beta$ phase is lower than in the $\alpha$ phase. In the presence of a single vacancy in the $\beta$ phase, $f$ does not depend on the vacancy composition for small vacancy concentrations, having a value of approximately 0.37. In Monte Carlo cells containing two vacancies, however, $f$ varies strongly with vacancy concentration, decreasing as the vacancy concentration increases. Hops between the nearest-neighbor octahedral sites in $\beta$-$Li_2Ti_2O_4$ are modeled within the kinetic Monte Carlo simulations as occurring in two steps through the in-

termediate tetrahedral site. The fact that the Li ions are assumed to thermalize in the tetrahedral sites increases the fraction of return hops to the initial octahedral site.

## IV. DISCUSSION

Intercalation compounds used as electrodes in Li-ion batteries come in a wide variety of crystal structures. The crystal structure of an intercalation compound can have a strong influence on the electrochemical properties of an electrode material, including the voltage profile and the concentration dependence of the Li-diffusion coefficient. Here we performed a comprehensive study of Li diffusion in the spinel crystal structure, focusing in particular on $Li_{1+x}Ti_2O_4$. The spinel crystal structure is more complex than many other intercalation compounds used as electrodes in Li-ion batteries in that it consists of both tetrahedral and octahedral sites that can be occupied by Li. Below $x=0$ in spinel $Li_{1+x}Ti_2O_4$, Li occupies the tetrahedral sites, while at $x=1$, Li occupies the more numerous but energetically less favorable octahedral sites. A miscibility gap exists between $x=0$ and $x=1$ due to the strong repulsion between pairs of Li ions occupying nearest-neighbor tetrahedral and octahedral sites. Spinel $Li_{1+x}Ti_2O_4$ is very similar in structure to the Li-excess spinel, $Li_{1+x}(Li_{1/6}Ti_{5/6})_2O_4$, an attractive anode material. Both the titanate spinel and its Li-excess variant exhibit the rare trait that their lattice parameters vary negligibly with Li concentration (between $x=0$ and 1), making them less susceptible than other intercalation compounds to mechanical degradation during Li removal and reinsertion. Our study of the titanate spinel also sheds light on diffusion mechanisms in $Li_xMn_2O_4$ spinel, although the existence of charge ordering over the Mn ions is likely to complicate Li transport in the Mn spinel.

While only a limited concentration interval is accessible experimentally below $x=0$ in $Li_{1+x}Ti_2O_4$, an advantage of a computational study is that it enables us to investigate the characteristics of Li diffusion within the spinel crystal structure even at concentrations where the host is metastable. Our study of Li diffusion for $x<0$ has yielded the surprising prediction that the octahedral sites, intermediate between neighboring tetrahedral sites, are in fact the transition states (i.e., saddle points on the energy surface) for elementary Li hops. This is in contrast to what has been predicted for the octahedral sites in the spinel form of $Li_{1+x}Mn_2O_4$, where the octahedral sites for $x<0$ are local minima.[58] Furthermore, we have found that the difference in energy between the octahedral site and the tetrahedral site decreases with increasing Li concentration $x$. Hence the migration barriers for elementary Li hops between tetrahedral sites decrease as more Li ions fill the tetrahedral sites. This trend does not arise solely from a change in crystal dimensions with Li concentration, as was predicted for the layered intercalation compounds.[6,7] The same trend was found when calculating the migration barriers at different concentrations while holding the supercell volume at each concentration fixed to a common value. The decrease in migration barrier with increasing Li concentration has an electrostatic origin, as an increase in the Li content leads to a progressive reduction of

the effective Ti valence from $Ti^{4+}$ at $x=-1$ to $Ti^{3.5+}$ at $x=0$. Indeed, we found that the difference between the electrostatic energy of Li in the octahedral site and the tetrahedral site decreases as the Ti valence decreases. We expect a similar trend in other spinels, including $Li_{1+x}Mn_2O_4$.

At $x=1$, where the Li ions occupy octahedral sites, diffusion becomes more complex. The tetrahedral sites between the nearest-neighbor octahedral sites are now local minima and hops between octahedral sites proceed in two steps. Furthermore, in the presence of a divacancy over octahedral sites, the intermediate tetrahedral site actually becomes more stable than the end states.

When serving as an anode, only the voltage plateau between $x=0$ and 1 in spinel $Li_{1+x}Ti_2O_4$ is cycled over. The plateau signifies two-phase coexistence between $LiTi_2O_4$ and $Li_2Ti_2O_4$ and the insertion or removal of Li ions from the two-phase mixture will require the migration of interfaces separating the coexisting phases. The kinetics of this process can be treated as a standard moving boundary problem,[59] where the velocity of the interface separating $LiTi_2O_4$ domains (tetrahedral occupancy) from $Li_2Ti_2O_4$ domains (octahedral occupancy) depends on the diffusion coefficients within the coexisting phases. Our study has shown that the diffusion coefficients of $LiTi_2O_4$ and $Li_2Ti_2O_4$ do not significantly differ from each other, in spite of the qualitative differences in hop mechanisms at the atomic scale for $x=0$ and $x=1$. If the interface between the coexisting phases has a sluggish mobility and thereby becomes the rate-limiting step of Li extraction and insertion, then additional kinetic coefficients relating interface velocity to differences in thermodynamic potentials across the interface must be determined. At this stage, our understanding of the mobility of interfaces in solids remains very limited.[60]

An important difference between the spinel crystal structure and the layered crystal structures of $Li_xCoO_2$, $Li_xTiS_2$ and $Li_x(Co_{1/3}Ni_{1/3}Mn_{1/3})O_2$ among others is the dimensionality of the interstitial network. The layered intercalation compounds limit Li diffusion to two-dimensional triangular lattices. Individual Li hops between neighboring octahedral sites of layered intercalation compounds pass through an adjacent tetrahedral site and the migration barriers for these hops are significantly reduced if they occur into a divacancy.[6,7] At high Li concentrations, the self- and tracer-diffusion coefficients therefore scale with the divacancy concentration, which to first order is equal to $x_V^2$ (where, $x_V$ is concentration of vacancies). In spinel $Li_{1+x}Ti_2O_4$ when $x<0$ in contrast, diffusion is mediated by a single vacancy mechanism such that the tracer and self-diffusion coefficients depend linearly on the vacancy concentration. The correlation factors of Li diffusion also differ substantially between layered intercalation compounds and spinel, with that of the spinel phase being a factor of 5–10 times larger than that of layered intercalation compounds at high Li concentrations.[6] The efficiency of redistributing Li ions through a divacancy mechanism over a two-dimensional network is significantly lower than through a single vacancy mechanism in a three-dimensional network. Hence for the same migration barrier for individual hops, the spinel crystal structure should offer Li ions a higher mobility (as measured by $D^*$ and $D_J$) compared to layered intercalation compounds.

The present study can be extended to the Li-excess variant, $Li_{1+x}(Li_{1/6}Ti_{5/6})_2O_4$, with similar methodological and computational infrastructure. In Li-excess spinel, the excess Li ions occupy a fraction of the Ti octahedral $16d$ sites. The Ti sublattice will then also exhibits configurational degrees of freedom arising from all possible ways of arranging Li and Ti. The additional configurational degrees of freedom can be treated with a coupled sublattice cluster expansion.[61,62]

## V. CONCLUSIONS

We have performed a first-principles investigation of the concentration dependent Li-diffusion coefficient in spinel $Li_{1+x}Ti_2O_4$ by applying kinetic Monte Carlo simulations to a first-principles cluster expansion of the configurational energy of Li-vacancy disorder over the interstitial sites of the $Ti_2O_4$ host. Spinel transition metal oxide intercalation compounds such as $Li_xMn_2O_4$ and $Li_{1+x}(Li_{1/6}Ti_{5/6})_2O_4$ are important electrode materials for Li-ion batteries. The present study has demonstrated that the octahedral sites are activated states for Li hops between neighboring tetrahedral sites when $x < 0$ in $Li_{1+x}Ti_2O_4$. Furthermore, the migration barriers for hops between neighboring tetrahedral sites are sensitive to Li concentration, decreasing with increasing $x$. We have been able to attribute this decrease with an increase in the effective Ti valence states as Li is added to the host, which penalizes the octahedral site more than the tetrahedral site. In $Li_2Ti_2O_4$, Li ions occupy octahedral sites and migrate by passing through intermediate tetrahedral sites, which are predicted to be locally stable (as opposed to being saddle points in the energy landscape). The predicted Li-diffusion coefficient varies by several orders of magnitude with Li concentration for $x < 0$. In spite of the qualitative difference in hop mechanisms in $LiTi_2O_4$ and $Li_2Ti_2O_4$, their Li-diffusion coefficients are nevertheless very similar in value. Our study provides insight about the effect of crystallographic features in spinel and layered intercalation compounds on Li mobility.

## ACKNOWLEDGMENTS

*Corresponding author. FAX: +001 7347634788; avdv@umich.edu

[1] M. S. Whittingham, Chem. Rev. **104**, 4271 (2004).

[2] C. Delmas, C. Fouassier, and P. Hagenmuller, Physica B & C **99**, 81 (1980).

[3] M. M. Thackeray, J. Electrochem. Soc. **142**, 2558 (1995).

[4] M. M. Thackeray, Prog. Solid State Chem. **25**, 1 (1997).

[5] A. Van der Ven and G. Ceder, J. Power Sources **97-98**, 529 (2001).

[6] A. Van der Ven, G. Ceder, M. Asta, and P. D. Tepesch, Phys. Rev. B **64**, 184307 (2001).

[7] A. Van der Ven, J. C. Thomas, Q. Xu, B. Swoboda, and D. Morgan, Phys. Rev. B **78**, 104306 (2008).

[8] A. K. Padhi, K. S. Najundaswamy, and J. B. Goodenough, J. Electrochem. Soc. **144**, 1188 (1997).

[9] D. Morgan, A. Van der Ven, and G. Ceder, Electrochem. Solid-State Lett. **7**, A30 (2004).

[10] G. Y. Chen, X. Y. Song, and T. J. Richardson, Electrochem. Solid-State Lett. **9**, A295 (2006).

[11] C. Delmas, M. Maccario, L. Croguennec, F. Le Cras, and F. Weill, Nature Mater. **7**, 665 (2008).

[12] N. Meethong, H. Y. S. Huang, S. A. Speakman, W. C. Carter, and Y. M. Chiang, Adv. Mater. **17**, 1115 (2007).

[13] A. Van der Ven, K. Garikipati, S. Kim, and M. Wagemaker, J. Electrochem. Soc. **156**, A949 (2009).

[14] M. M. Thackeray, W. I. F. David, P. G. Bruce, and J. B. Goodenough, Mater. Res. Bull. **18**, 461 (1983).

[15] F. Bonino, L. Busani, M. Lazzari, M. Manstretta, B. Rivolta, and B. Scrosati, J. Power Sources **6**, 261 (1981).

[16] T. Ohzuku, T. Kodama, and T. Hirai, J. Power Sources **14**, 153 (1985).

[17] D. W. Murphy, R. J. Cava, S. M. Zahurak, and A. Santoro, Solid State Ionics **9-10**, 413 (1983).

[18] R. J. Cava, D. W. Murphy, S. Zahurak, A. Santoro, and R. S. Roth, J. Solid State Chem. **53**, 64 (1984).

[19] K. M. Colbow, J. R. Dahn, and R. R. Haering, J. Power Sources **26**, 397 (1989).

[20] J. M. Tarascon, E. Wang, F. K. Shokoohi, W. R. McKinnon, and S. Colson, J. Electrochem. Soc. **138**, 2859 (1991).

[21] J. Rodriguez-Carvajal, G. Rousse, C. Masquelier, and M. Hervieu, Phys. Rev. Lett. **81**, 4660 (1998).

[22] A. Yamada and M. Tanaka, Mater. Res. Bull. **30**, 715 (1995).

[23] J. E. Greedan, N. P. Raju, A. S. Wills, C. Morin, S. M. Shaw, and J. N. Reimers, Chem. Mater. **10**, 3058 (1998).

[24] J. E. Greedan, C. R. Wiebe, A. S. Wills, and J. R. Stewart, Phys. Rev. B **65**, 184424 (2002).

[25] Y. I. Jang, B. Huang, F. C. Chou, D. R. Sadoway, and Y. M. Chiang, J. Appl. Phys. **87**, 7382 (2000).

[26] M. Wagemaker, A. Van der Ven, D. Morgan, G. Ceder, F. M. Mulder, and G. J. Kearley, Chem. Phys. **317**, 130 (2005).

[27] E. Ferg, R. J. Gummow, A. Dekock, and M. M. Thackeray, J. Electrochem. Soc. **141**, L147 (1994).

[28] T. Ohzuku, A. Ueda, and N. Yamamoto, J. Electrochem. Soc. **142**, 1431 (1995).

[29] K. Zaghib, M. Simoneau, M. Armand, and M. Gauthier, J. Power Sources **81-82**, 300 (1999).

[30] S. Scharner, W. Weppner, and P. Schmid-Beurmann, J. Electrochem. Soc. **146**, 857 (1999).

[31] P. Arora, R. E. White, and M. Doyle, J. Electrochem. Soc. **145**, 3647 (1998).

[32] S. S. Zhang, M. S. Ding, K. Xu, J. Allen, and T. R. Jow, Electrochem. Solid-State Lett. **4**, A206 (2001).

[33] J. Hafner, C. Wolverton, and G. Ceder, MRS Bull. **31**, 659 (2006).

[34] J. M. Sanchez, F. Duscastelle, and D. Gratias, Physica A **128**, 334 (1984).

[35] D. de Fontaine, Solid State Phys. **47**, 33 (1994).

[36] A. Van der Ven and G. Ceder, *Handbook of Materials Modeling*, Methods and Models Vol. 1, edited by R. Catlow, H. Shercliff, and S. Yip (Kluwer, Dordrecht, 2005).

[37] A. Van der Ven, H. C. Yu, G. Ceder, and K. Thornton, Prog. Mater. Sci. **55**, 61 (2010).

[38] G. Kresse and J. Furthmuller, Phys. Rev. B **54**, 11169 (1996).

[39] G. Kresse and J. Furthmuller, Comput. Mater. Sci. **6**, 15 (1996).

[40] P. E. Blöchl, Phys. Rev. B **50**, 17953 (1994).

[41] G. Kresse and D. Joubert, Phys. Rev. B **59**, 1758 (1999).

[42] D. B. Laks, L. G. Ferreira, S. Froyen, and A. Zunger, Phys. Rev. B **46**, 12587 (1992).

[43] A. van de Walle and G. Ceder, J. Phase Equilib. **23**, 348 (2002).

[44] G. L. W. Hart, V. Blum, M. J. Walorski, and A. Zunger, Nature Mater. **4**, 391 (2005).

[45] R. Gomer, Rep. Prog. Phys. **53**, 917 (1990).

[46] P. M. Richards, Phys. Rev. B **16**, 1393 (1977).

[47] A. B. Bortz, M. H. Kalos, and J. L. Lebowitz, J. Comput. Phys. **17**, 10 (1975).

[48] F. M. Bulnes, V. D. Pereyra, and J. L. Riccardo, Phys. Rev. E **58**, 86 (1998).

[49] G. H. Vineyard, J. Phys. Chem. Solids **3**, 121 (1957).

[50] E. Moshopoulou, P. Bordet, J. J. Capponi, C. Chaillout, B. Souletie, and A. Sulpice, J. Alloys Compd. **195**, 81 (1993).

[51] G. Ceder, G. D. Garbulsky, and P. D. Tepesch, Phys. Rev. B **51**, 11257 (1995).

[52] F. Zhou, M. Cococcioni, K. Kang, and G. Ceder, Electrochem. Commun. **6**, 1144 (2004).

[53] A. van de Walle and M. Asta, Modell. Simul. Mater. Sci. Eng. **10**, 521 (2002).

[54] A. F. Kohan, P. D. Tepesch, G. Ceder, and C. Wolverton, Comput. Mater. Sci. **9**, 389 (1998).

[55] M. Wagemaker, E. R. H. van Eck, A. P. M. Kentgens, and F. M. Mulder, J. Phys. Chem. B **113**, 224 (2009).

[56] R. LeSar, R. Najafabadi, and D. J. Srolovitz, Phys. Rev. Lett. **63**, 624 (1989).

[57] K. Compaan and Y. Haven, Trans. Faraday Soc. **52**, 786 (1956).

[58] C. Y. Ouyang, S. Q. Shi, Z. X. Wang, H. Li, X. J. Huang, and L. Q. Chen, Europhys. Lett. **67**, 28 (2004).

[59] S. Crusius, G. Inden, U. Knoop, L. Hoglund, and J. Agren, Z. Metallkd. **83**, 673 (1992).

[60] M. Hillert, Acta Mater. **47**, 4481 (1999).

[61] P. D. Tepesch, G. D. Garbulsky, and G. Ceder, Phys. Rev. Lett. **74**, 2272 (1995).

[62] J. C. Thomas, J. M. Millunchick, N. A. Modine, and A. Van der Ven, Phys. Rev. B **80**, 125315 (2009).